LEVEL II

SGI-R-79-003

B.S.

SEISMIC STUDIES OF THE NEVADA TEST SITE

DAVID M. HADLEY

ROBERT S. HART

QUARTERLY TECHNICAL REPORT

FOR PERIOD FEBRUARY 1 - MAY 31, 1979

SPONSORED BY

DEFENSE ADVANCED RESEARCH PROJECTS AGENCY (DOD)

ARPA ORDER NO. 2551

This research was supported by the Advanced Research Projects Agency of the Department of Defense and was monitored by AFTAC/VSC, Patrick AFB, Fl. 32925, under Contract No. F08606-79-C-0009.

June 1979

SIERRA GEOPHYSICS, INC.

150 N. SANTA ANITA AVENUE • ARCADIA, CALIFORNIA 91006 • (213) 574-7052

AFTAC Project Authorization: VT/9710

ARPA Order: 2551

Effective Date of Contract: November 22, 1978

Contract Expiration Date: September 30, 1979

Contract No: F08606-79-0009

Principal Investigators and Phone No:

Dr. Robert S. Hart

Dr. David M. Hadley

Dr. Rhett Butler

(213) 574-7052

Program Manager and Phone No:

Mr. Michael J. Shore

(202) 325-7581

SGI-R-79-003

SEISMIC STUDIES OF THE NEVADA TEST SITE

David M. Hadley

Robert S. Hart

Quarterly Technical Report

For Period February 1 - May 31, 1979

Sponsored By

Defense Advanced Research Projects Agency (DOD)

ARPA Order No. 2551

This research was supported by the Advanced Research Projects Agency of the Department of Defense and was monitored by AFTAC/VSC, Patrick AFB, Fl. 32925, under Contract No. F08606-79-C-0009.

June 1979

Unclassified

SECURITY CLASSIFICATION OF THIS PAGE (When Data Entered)

REPORT DOCUMENTATION PAGE

READ INSTRUCTIONS BEFORE COMPLETING FORM

1. REPORT NUMBER

2. GOVT ACCESSION NO.

3. RECIPIENT'S CATALOG NUMBER

4. TITLE (and Subtitle)

(6) Seismic Studies of the Nevada Test Site.

5. TYPE OF REPORT & PERIOD COVERED
Quarterly Technical
2/1/79 - 5/31/79

6. PERFORMING ORG. REPORT NUMBER
(14) SGI-R-79-003

7. AUTHOR(s)

(10) David M. Hadley
Robert S. Hart

8. CONTRACT OR GRANT NUMBER(s)
Contract No.
F08606-79-C-0009

9. PERFORMING ORGANIZATION NAME AND ADDRESS
Sierra Geophysics, Inc.
150 N. Santa Anita Ave.
Arcadia, CA 91006

10. PROGRAM ELEMENT, PROJECT, TASK AREA & WORK UNIT NUMBERS
ARPA Order No. 2551

11. CONTROLLING OFFICE NAME AND ADDRESS
VELA Seismological Center
312 Montgomery Street
Alexandria, VA 22314

(11) 12. REPORT DATE
June 1979

13. NUMBER OF PAGES
44

14. MONITORING AGENCY NAME & ADDRESS (if different from Controlling Office)
(15) F08606-79-C-0009,
ARPA Order-2551

15. SECURITY CLASS. (of this report)
Unclassified

15a. DECLASSIFICATION/DOWNGRADING SCHEDULE

16. DISTRIBUTION STATEMENT (of this Report)

Approved for public release, distribution unlimited (12) 50

17. DISTRIBUTION STATEMENT (of the abstract entered in Block 20, if different from Report)

(9) Quarterly technical rept.
1 Feb - 31 May 79,

18. SUPPLEMENTARY NOTES

19. KEY WORDS (Continue on reverse side if necessary and identify by block number)
Receiver structure
Attenuation
Piledriver Hard Hat
Seismic Wave Propagation
Heterogeneous Media
Reduced Displacement Potentials
IN THIS REPORT,

20. ABSTRACT (Continue on reverse side if necessary and identify by block number)

Results are presented from research conducted during the period March - May, 1979. The following three areas are discussed: 1) Geological and exploration geophysical data for the Yucca Flats area of NTS have been used to develop 3-dimensional models for studies of wave propagation in that basin. Amplitude and waveform complexity is examined for both incoming and outgoing seismic rays as a function of both azimuth and location across the basin. For the incoming case, the direct arrival is only minimally

DD FORM 1 JAN 73 1473 EDITION OF 1 NOV 65 IS OBSOLETE

Unclassified

SECURITY CLASSIFICATION OF THIS PAGE (When Data Entered)

393 821

affected by changes in either azimuth or station location. The amplitude and timing of the secondary arrivals are very sensitive to such changes. For the outgoing case, substantial changes (a factor of 2-3) in amplitude can be obtained both as the azimuth changes and as the source location is shifted a small distance (2-3km) across the basin.

2. Through a deconvolution of teleseismic waveforms recorded at Climax Stock from the waveforms recorded at Yucca Flats an estimation of the receiver function for the sedimentary basin can be obtained. This receiver function is interpreted as a series of pulses that represent the timing, amplitude and polarity of multiple bounces within the sedimentary structure. For outgoing energy, the phase pP shares much of the same path traversed by the first multiple for incoming energy. Distortion of the phase pP and the addition of pulses representing energy that bounces within the basin will strongly modify the teleseismic waveforms and m_b measurements.

3. This report is the second part of a continuing project to define both the teleseismic path averaged attenuation operator appropriate for sources located at NTS and the deviation from the average associated with distinct geologic structures. In the following sections we will interrelate: (1) near-field data from Piledriver; (2) scaling relations for a 62kt source. (3) teleseismic WWSSN waveforms for Piledriver; (4) regional amplitude data from Piledriver; (5) RDP's from Hard Hat; and (6) regional amplitude data from Hard Hat. Unfortunately, these six data sets are not internally consistent. Therefore the results must depend, to some extent on which data are heavily weighted in the analysis.

TABLE OF CONTENTS

I. INTRODUCTION

The objective of the research program underway at Sierra Geophysics on behalf of AFTAC/VSC is to examine and interpret the causes of the observed m_b yield biases observed at the Nevada Test Site (NTS). The first part of this program involves the analysis of short period seismic energy radiated from tests at NTS and of teleseisms recorded at the SDCS stations located throughout NTS. The second task of the overall program is the collection and synthesis of the available geological and geophysical data pertaining to the crustal structure at NTS followed by the modeling of seismic propagation through those structures. Finally, the results of the above two tasks will be integrated to relate the inferred seismological structure with that predicted from the geologic and exploration geophysics. In conjunction with this last task, studies will be made regarding the sensitivity of the observed seismic energy to variations of structural parameters with the goal of estimating the quality of the geologic and geophysical data necessary to define a useful transfer function for the site.

This report summarizes the work done in these areas during the second quarterly period of the current contract.

II. RESEARCH SUMMARY

Our research during this quarter can be divided into three

specific areas of inquiry. These are; (1) wave propagation studies that incorporate the Yucca Flats structure for both incoming and outgoing seismic energy; (2) deconvolution studies for the estimation of receiver structure from teleseisms records at the Yucca Flats and Climax Stock SDCS stations, and (3) modeling of the reduced displacement potential (RDP) and teleseismic attenuation (t*) for outgoing energy from the Piledriver event at Climax Stock. Each of these will be treated separately in the following text. It should be emphasized, however, that the first two topics to be discussed (Sections 1 and 2) below, represent status reports on ongoing research.

1. Model Studies of Yucca Flats

The modeling of Yucca Flats has centered around an east-west structural profile, Figure 1.1, produced by Gene Herrin under a current AFOSR research contract. Additional data and maps from the U.S. Geological Survey and Herrin (personal communication) were used to extend this cross section north and south to obtain a three-dimensional model for the region. However, the profile shown in Figure 1.1 was particularly important since it is quite near the SDCS stations (YF-NV, YF2-NV, YF3-NV, and YF4-NV). Several teleseismically recorded tests were also located close to this profile.

The first procedure followed has been the modeling of incoming seismic energy recorded by the YF array. This procedure has examined waveform complexity and amplitude variations both with changing azimuth and with station position across the valley. Additional studies have been made on the effects of changing major morphological features of the basin.

In Figure 1.2, we illustrate the results of a study of incoming seismic energy for the basin structure shown in Figure 1.1. We have plotted the theoretical seismograms which would be observed at four separate sites across the basin (rows 1, 2, 3, and 4 in the figure) which correspond to the positions of stations YF4-NV, YF3-NV, YF2-NV, and YF-NV respectively. Each column of seismograms illustrates the waveforms for a particular back azimuth (E, W, N, SE, and NW). The seismograms

East-West Profile Across Yucca Valley at 37 deg 1.6min North

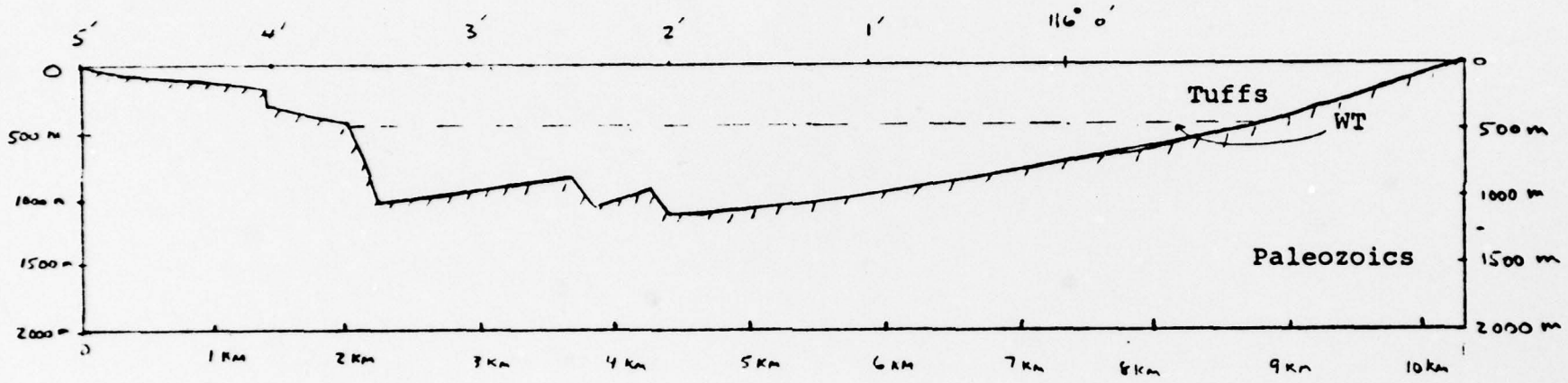

Figure 1.1

Approximate velocities:

Tuffs above Water Table	1.5 Km/sec	density 2.0
Tuffs below Water Table	2.4 Km/sec	density 2.2
Paleozoics	5.0 Km/sec	density 2.6

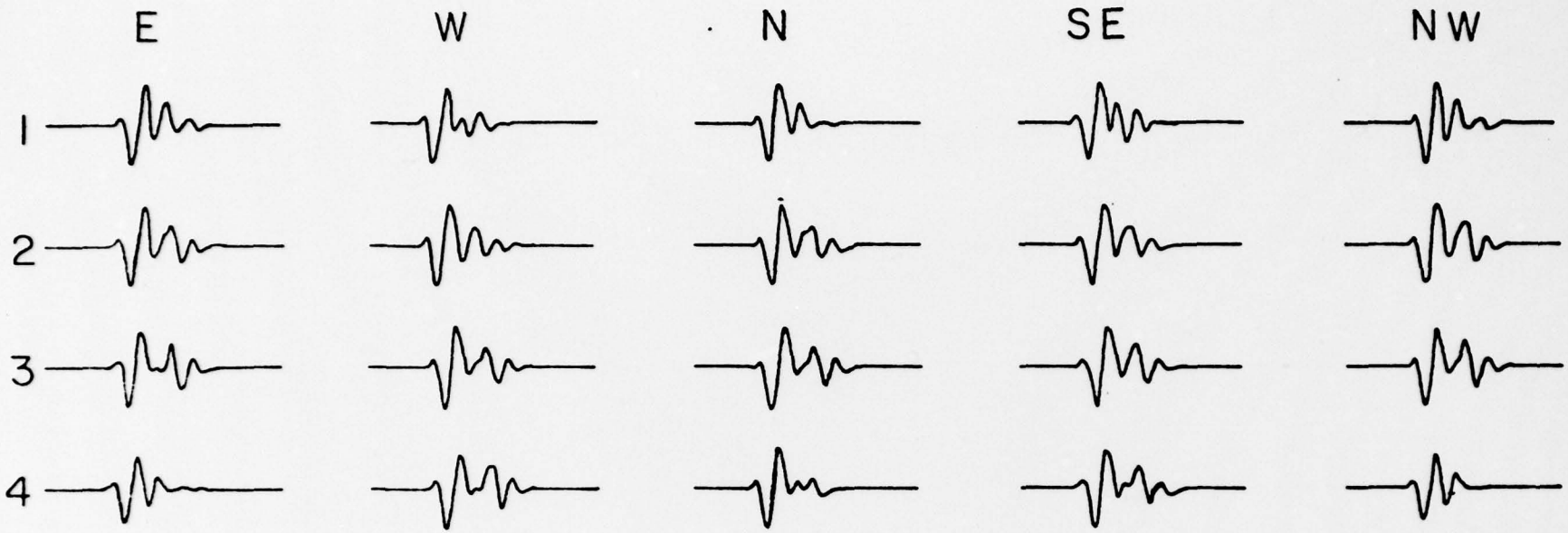

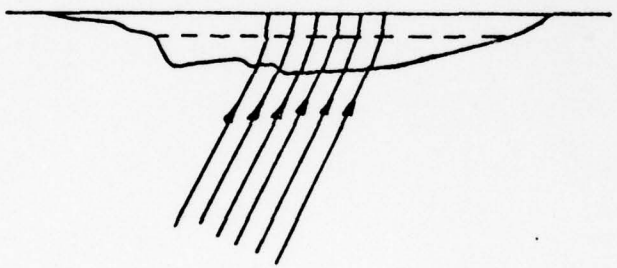

Figure 1.2. Very short period incoming waveforms for various back azimuth and station locations across the Yucca Valley basin. Rows 1 through 4 correspond to the positions of SDCS stations YF4NV, YF3NV, YF2NV, and YFNV respectively.

have been computed by convolving the delta function arrivals with a very short period doublet (duration ~ 1.0 seconds) that represents an approximation to the source, Q, and instrument effects. This short period function was chosen in order to more clearly separate the individual arrivals for discussion purposes. In an actual recording, these phases would interfere causing modulations in the observed seismogram. We can draw several important conclusions from the information present on this figure. The direct ray is, as would be anticipated, only minimally affected by changes in either azimuth or station location. The amplitude and timing of the secondary arrivals, whose paths are analogous to a pP phase from a source in the basin, are very sensitive to such changes. Fairly small azimuthally dependent changes are seen for station 1 near the basin center. However, as the observation point is moved closer to the sides of the basin, azimuthal variations in the secondary phases become pronounced.

The interference effects of these secondary arrival variations are more clearly illustrated in the analysis of outgoing energy. In this example, we have included just 4 compressional rays leaving a surface focus source at Yucca Flats. These rays, illustrated in Figure 1.3, are the direct ray, the multiple reflected from the basin bottom and underside of the water table, the multiple reflected from the bottom of the basin and the

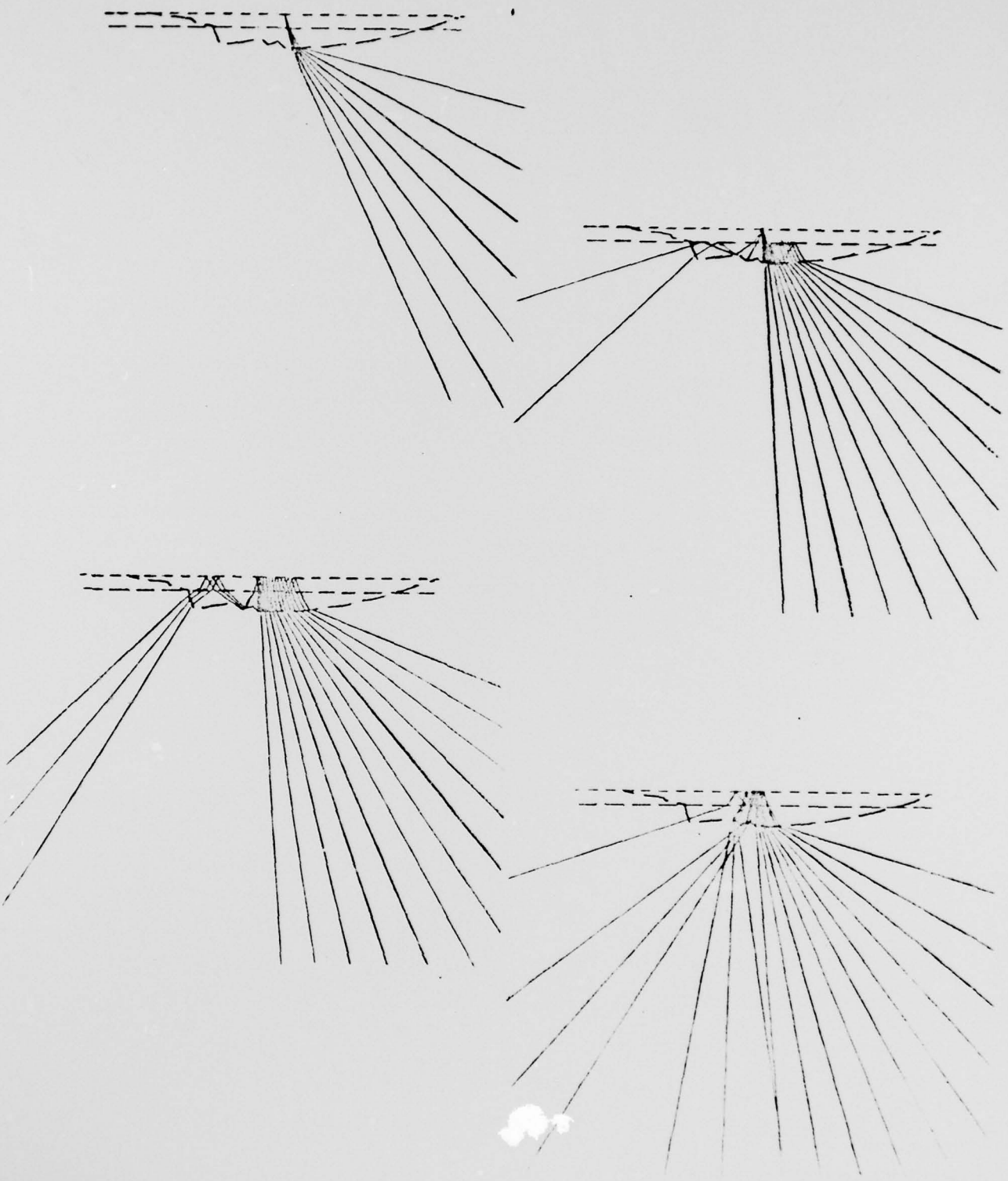

Figure 1.3. Ray paths for the first 4 outgoing P-wave multiples for a surface source at Yucca Flats.

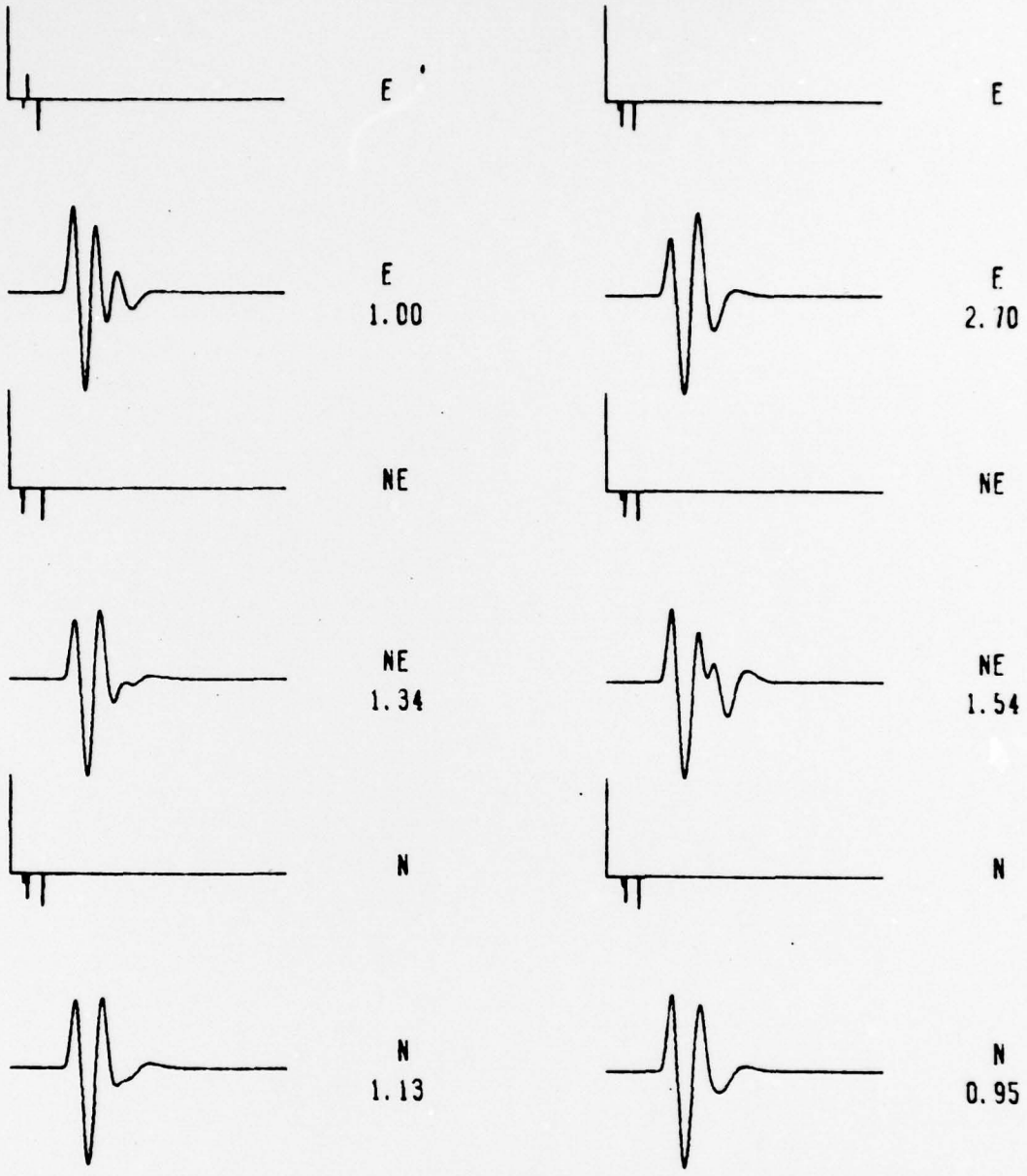

Figure 1.4. Delta function responses and predicted waveforms and amplitudes for two sources located at Yucca Flats as would be observed at a distance of 30° on a HNME-type short period instrument. The left-hand column illustrates three azimuthally different synthetics for a surface focus source at the center of the basin. The right-hand column shows the same stations for a source 1 kilometer east of the center. All waveform amplitudes have been normalized to the top left-hand synthetic.

free surface, and the ray reflected from the top of the water table and the free surface. We have computed these rays for a ray parameter appropriate for a distance of 30° and at several azimuths. The eastern, northeastern, and northern azimuths results are shown in Figure 1.4. The synthetics shown in that figure represent the convolution of the delta function responses at 30° with a HNME-type short period instrument response, with a von Seggern and Blandford (1972) source, and with a Q operator ($t^* = 1.0$). The lefthand column shows the seismograms from a source at the center of the Yucca Flats structure (Figure 1.1), the right hand column illustrates the seismograms originating from a source 1 km east of the center. The amplitudes of all six seismograms are normalized to the top left record (a record observed to the east from a center source). Also plotted above each seismogram is the delta function response at each station. Substantial changes, as much as a factor of 3, in amplitude can be obtained both as the azimuth changes and as the source location is shifted a fairly small distance across the basin.

Modeling efforts are continuing for both the incoming and outgoing cases. In particular, we are considering the outgoing case for sources buried at depths corresponding to Yucca Flats test depths.

2. Estimates of the Waveform Complexity and Amplitude Bias Introduced By Geologic Structure at Yucca Flats - A Comparison Between Energy Recorded at OB and YF Arrays

2.1 Introduction

Through a deconvolution of teleseismic waveforms recorded at Climax Stock, from the waveforms recorded at Yucca Flats, an estimation of the receiver function for the sedimentary basin can be obtained. This receiver function is interpreted as a series of pulses that represent the timing, amplitude and polarity of multiple bounces within the sedimentary structure. From reciprocity, the multiple bounces within the sedimentary structure, for the case of incoming energy, should characterize the complexity seen teleseismically for sources located within the basin. Distortion of the phase pP and the addition of pulses representing energy that bounces within the basin will strongly modify the teleseismic waveforms. In general, the phase pP constructively interfers with the backswing of the impulse response of the instrument. Hence, distortion of this phase can introduce a significant bias in the m_b measurement.

2.2 Deconvolution Techniques

Conceptually, the deconvolution of seismic tract, $S_1(t)$, from another, $S_2(t) = S_1(t) * T(t)$ where $T(t)$ is the transfer function for the two waveforms, is straightforward. Unfortunately, in the presence of noise the process is well known to be unstable. We

have developed a method for stacking the ratio $[S(\omega)\cdot T(\omega)]/S(\omega)$ that eliminates the noise as $\sqrt{n}$. This technique is similar, in some respects, to stacking complex cepstrum.

The examples of the data set to be used in this deconvolution technique are shown in Figures 2.1, 2.2, and 2.3. The traces on the left are from teleseismic P-waves recorded at the Climax Stock station OB2NV. For many deep-focus earthquakes, the seismograms at OB2NV look like a delta function convolved with just a Q operator and the instrument. In the following discussions we assume that the record at OB2NV is described by Source * Q * Instrument * Noise. The data collected at Yucca Flats, YF, are shown as a broken line on the right side of Figures 2.1, 2.2, and 2.3. Clearly the Yucca Valley sedimentary basin severely distorts, amplifies and prolongs the coda for the input signal. For each small range of azimuths and incidence angles, some transfer function should exist such that the record at YFNV can be constructed from OB2NV, i.e. YFNV = OB2NV * Transfer-function * Noise. This transfer-function, $\bar{T}(t)$, carries information about the arrival time and amplitude of first, second and later multiple bounces in the sedimentary basin.

To estimate this transfer function we have cosine windowed 6 seconds of data from OB2NV and 12 seconds of data from YFNV for a selection of events that arrive at NTS from approximately the same azimuth. Next, for each OB2NV-YFNV pair, the Fourier transform of the windowed data and the ratio of these transforms

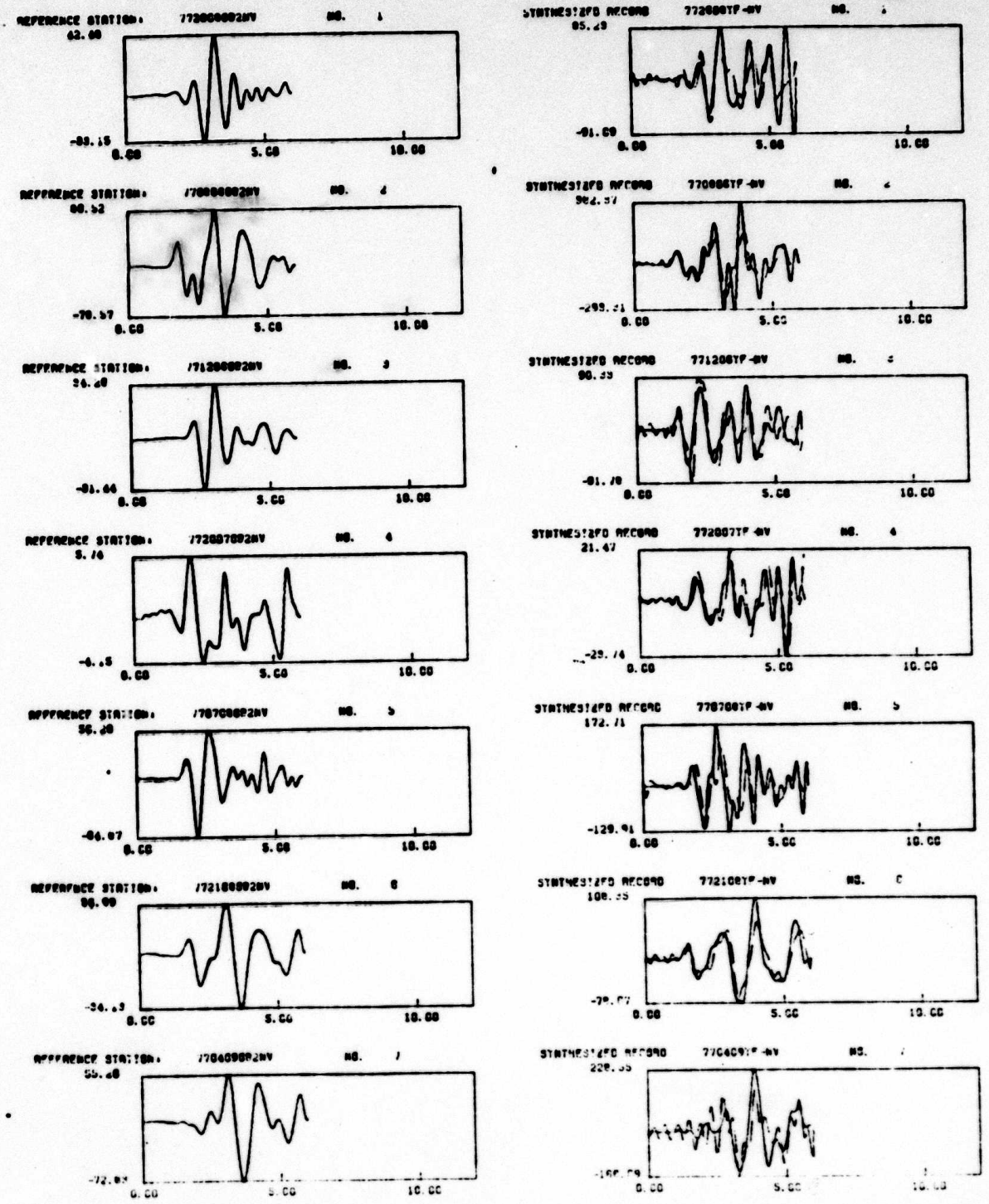

Figure 2.1a. For each teleseism, OB2NV (left column) was deconvolved from YFNV (right column - broken line) and the average transfer function $\bar{T}(t)$ was reconvolved with OB2NV (right column - solid line) - northwest azimuth. Six seconds of OB2NV data and 12 sec of YFNV and 14 teleseism pairs were used in the estimate of $\bar{T}(t)$.

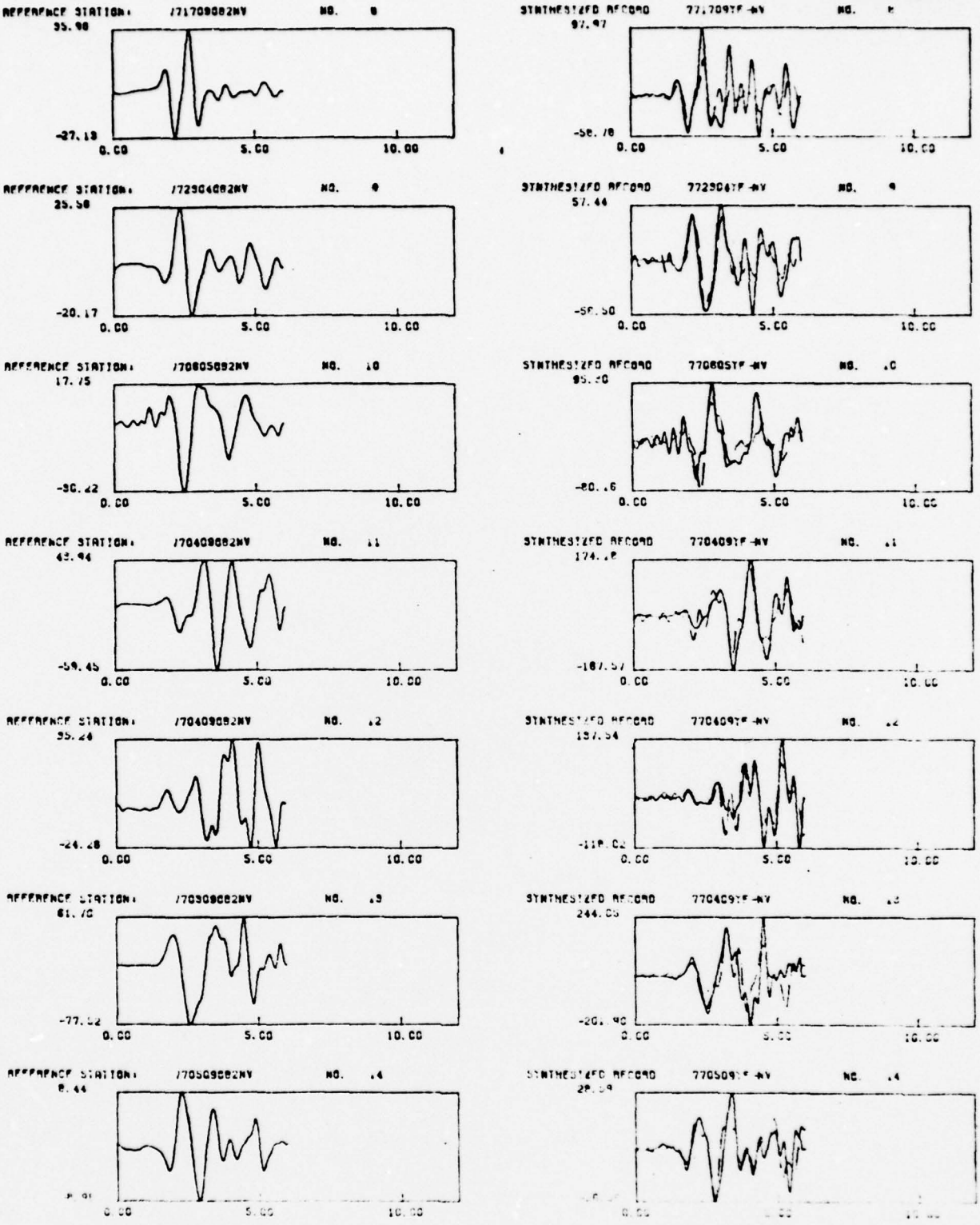

Figure 2.1b Continued

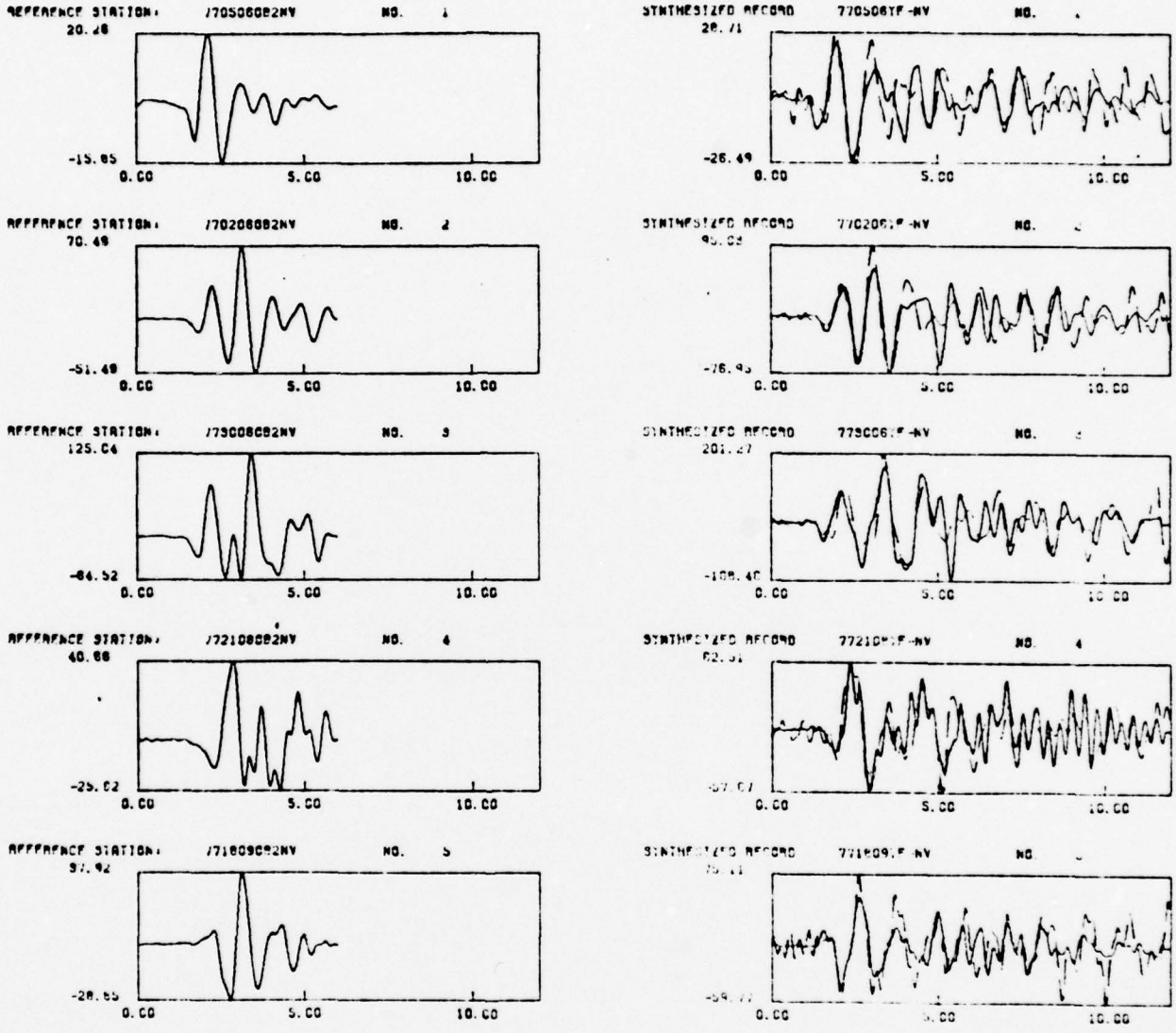

Figure 2.2. For each teleseism, OB2NV (left column) was deconvolved from YFNV (right column - broken line) and the average transfer function $\bar{T}(t)$ was reconvolved with OB2NV (right column - solid line) - southeast azimuth. Six seconds of OB2NV data and 12 seconds of YFNV data and 5 teleseism pairs were used in the estimate of $\bar{T}(t)$.

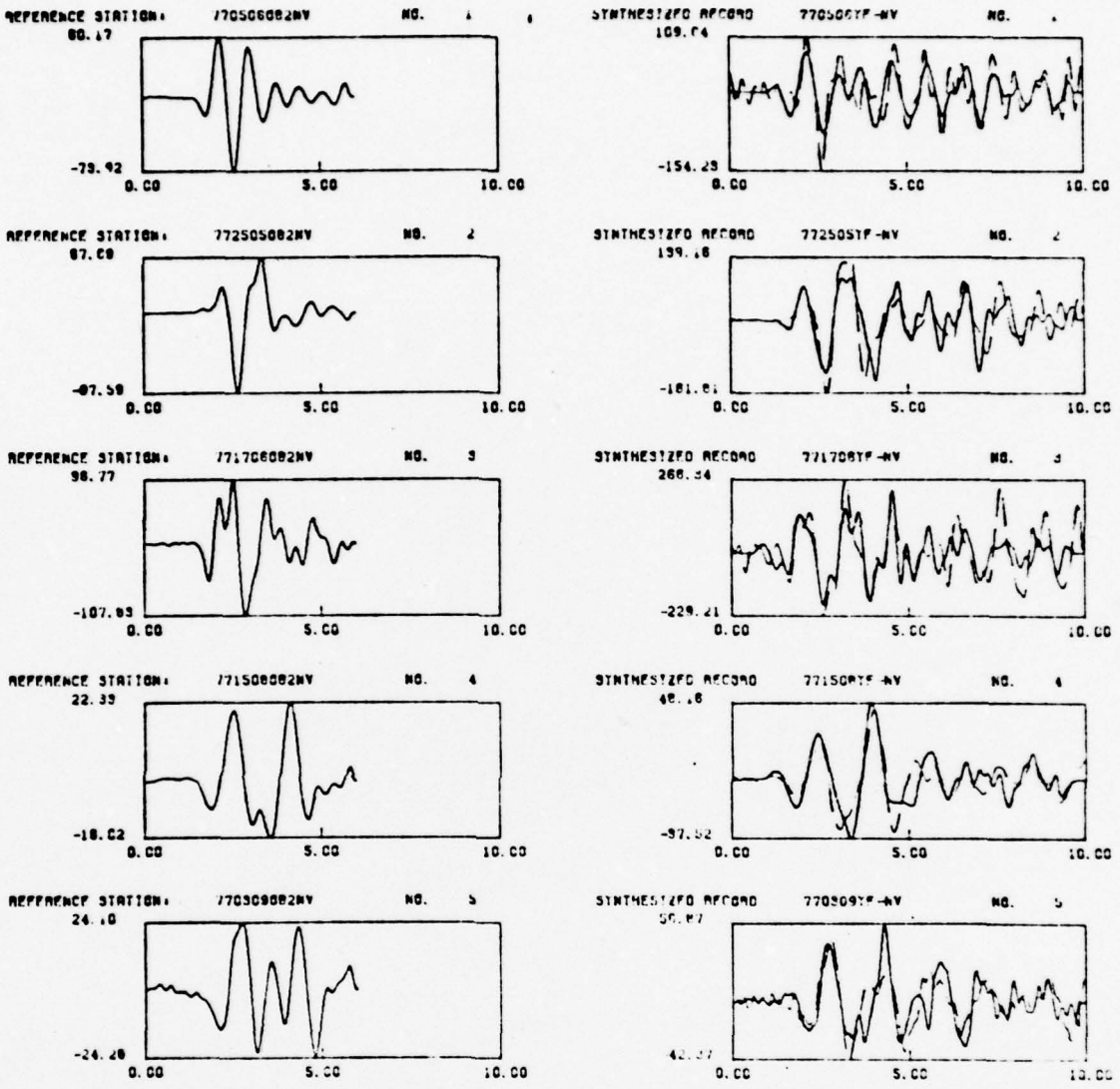

Figure 2.3. For each teleseism, OB2NV (left column) was deconvolved from YFNV (right column - broken line) and the average transfer function $\bar{T}(t)$ was reconvolved with OB2NV (right column - solid line) - southwest azimuth. Six seconds of OB2NV data and 12 seconds of YFNV data and 5 teleseism pairs were used in the estimate $\bar{T}(t)$.

are computed. For each earthquake, this ratio should be a noisy estimate of the transfer function. By stacking the log of the spectrum of many estimates we obtain:

$$\bar{T}(\omega) = \frac{1}{n} \Sigma\ T(\omega) + \frac{1}{n} \Sigma\ \text{noise} \qquad (2.1)$$

As n increases, the noise should decrease approximately as $\sqrt{n}$.

Stacking the log of the spectrum requires close attention to details. Two errors frequently occur in the unwinding and stacking of phase spectrum. The first frequent error occurs in making the phase continuous. Although the process ultimately amounts to adding or substracting multiples of 2π, the process should be invariant to linear shifts in time. In other words, if the trend of the phase spectrum is modified, equivalent to introducing a time shift Δt, the direction of the 2π jump should remain invariant. Most of the additions of 2π can be made with great confidence. The problem occurs around π phase jumps. We handle this problem by first oversampling the signal, typically five times the Nyquist frequency, in order to interpolate the phase spectrum. Second, we compute the local slope on both sides of a π jump and include the average slope in the decision to add or subtract 2π. After unwrapping the phase, we detrend the phase spectrum and adjust all detrended phase spectrums by multiples of 2π so that the differences of the means for all phase spectrums are minimized. The reason for performing this phase level equalization is easily seen with a simple example.

Consider unwinding four phase spectrums and suppose the first point is $-\frac{\pi}{2} \sim \delta$. The unwrapped spectrums should have about the same shape but one or more may be different by 2π. If, for example, one differs by 2π then the average phase is $\frac{1}{4} \times \Sigma$ phase + 90°, and the final stacked signal is Hilbert transformed (Choy and Richards, 1975). Without careful equilization, the stacked output will, in general, be phase shifted some unknown amount $2\pi m/n$.

2.3 Data Analysis and Discussion

For each of the three data sets shown in Figures 2.1, 2.2 and 2.3, an averaged transfer function $\bar{T}(t)$ was obtained. This function was then reconvolved with each OB2NV record and plotted as a solid line on the right side of each Figure. The good comparison between the predicted YFNV waveform and the observed (broken line), both in terms of amplitude and complexity, indicates that a stable estimate of $\bar{T}(t)$ can be obtained for each azimuth window. The estimation procedure for a receiver function at YFNV can be extended to world-wide stations. These functions could then be incorporated into source studies in order to obtain a better, or more noise free, estimate of the source.

The traces shown in Figure 2.4, are the low pass filtered transfer functions, $\bar{T}(t)$ used in the prediction of the YFNV waveforms. The largest number of earthquakes recorded with the SDCS NTS array are located along a great circle azimuth extending northwest from NTS. These earthquakes are typically deep and the waveforms are not complicated by multiple phases. The top

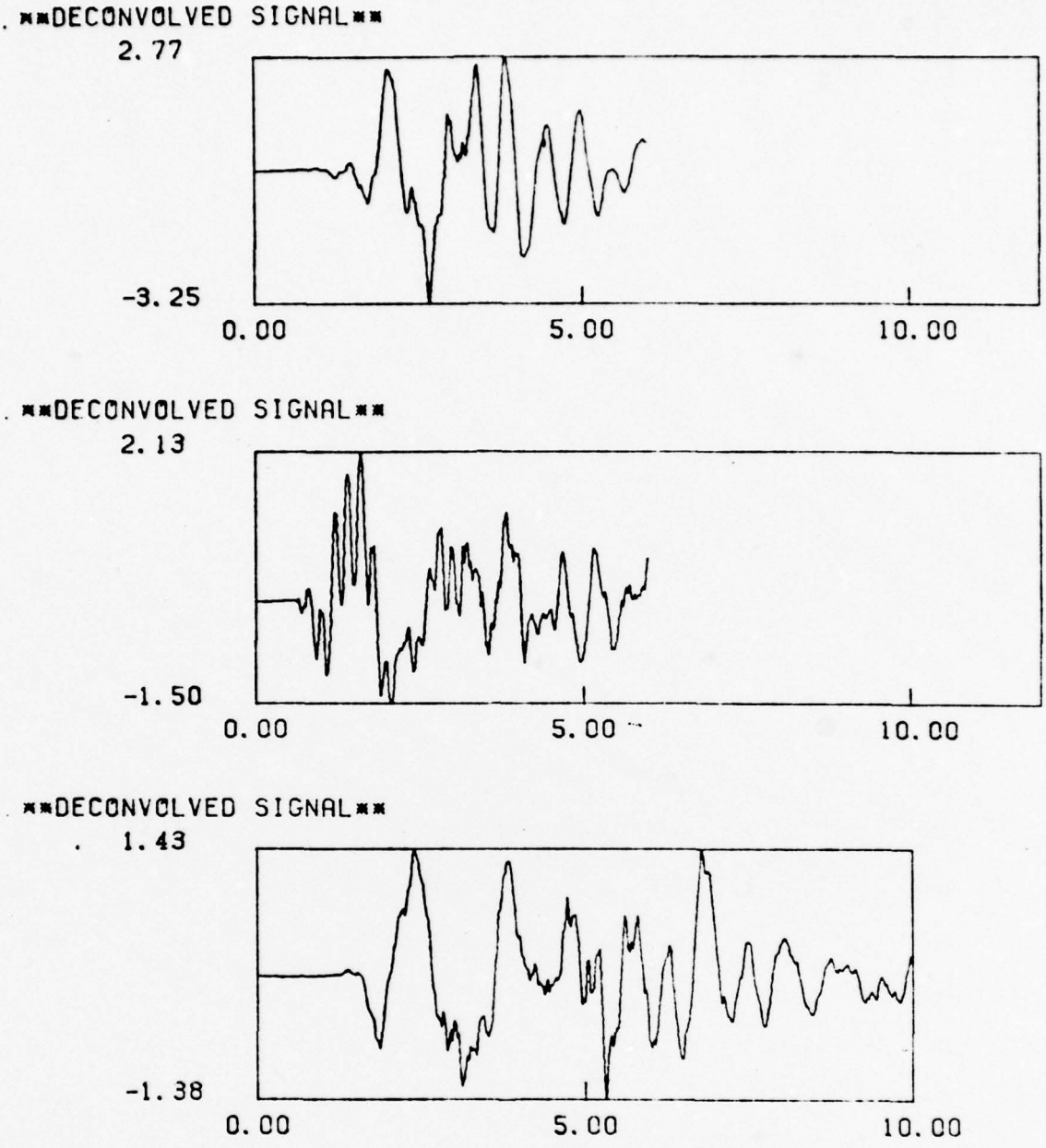

Figure 2.4. Low pass filtered average transfer function, $\bar{T}(t)$ for northwest (top), southeast (middle) and southwest (bottom) azimuths. Although the last two functions predict fairly well the amplitude and complexity of the waveforms for YFNV, see Figures 2.2 and 2.3., noise and the restricted data set have limited the estimate of $\bar{T}(t)$. This limitation introduces the slightly non-causal first downswing. The average transfer function, $\bar{T}(t)$, can be interpreted as representing the amplitude and the arrival time at YFNV of multiply reflected waves within the Yucca Flats sedimentary basin.

trace of Figure 2.4 is the low pass filter transfer function for this azimuth. The first major upswing is the first arrival. The second and even larger downswing is interpreted as the first multiple within the sedimentary basin. The modeling studies for Yucca Flats, discussed in other sections of this report, show that geologic structure can very effectively focus or defocus seismic energy. The strength of the second arrival, which is actually stronger than the first, requires a focusing phenomena.

The second and third traces in Figure 2.4 are for southeast and southwest azimuths respectively. These transfer functions have been estimated from a more limited data set and are somewhat noisier. As with the transfer function for the northwest azimuth, multiple bounces within the Yucca Flat basin introduce significant complexity into these transfer functions.

From a consideration of reciprocity, severe distortion of the incoming teleseismic energy at Yucca Flats implies distortion of outgoing energy from nuclear tests. Since many of the tests are located beneath the water table and near the bed rock interface, distortion of the direct arrivals should not be too severe. However, the upgoing phase pP will experience both focusing and defocusing. In addition multiple bounces within the basin will prolong the teleseismic coda. An example of this anticipated effect is seen in the teleseismic waveform comparisons of Piledriver, Jorum and Commodore, Figure 2.5. Stations ARE, KIP and

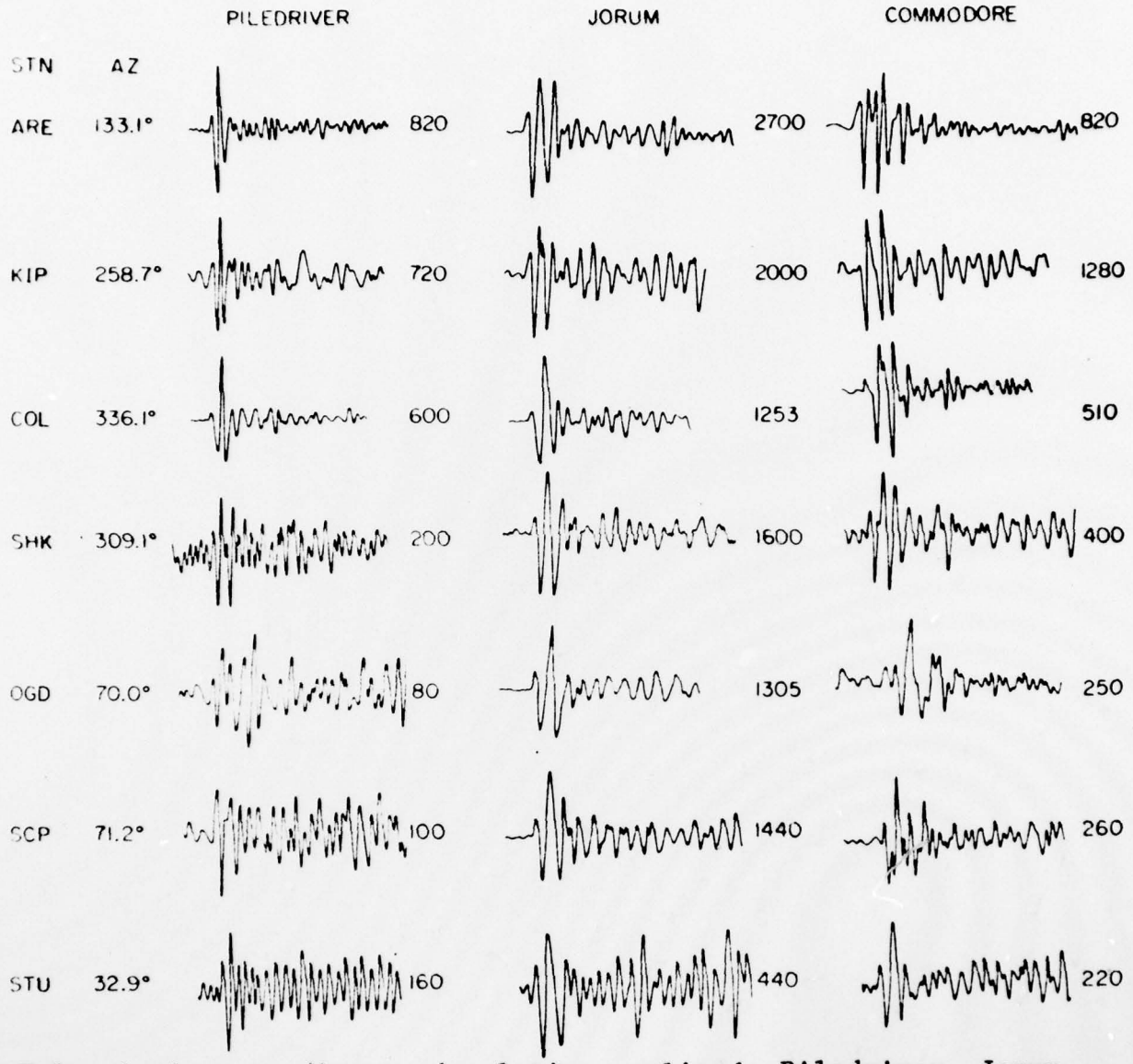

Figure 2.5. Teleseismic recordings and relative amplitudes Piledriver, Jorum, and Commodore. For the first three stations for Piledriver and the first six stations for Jorum, little complexity in the waveforms or attenuation of the amplitude is observed. This is interpreted as indicative of relatively simple source and receiver structure. By comparison with Piledriver and Jorum, multiple arrivals are clearly visible in the records from Commodore and must therefore be the result of structure at the source.

COL show very simple waveforms for Piledriver and Jorum. However, the multiple bounces that occur at the source are easily seen in the Commodore record. Distortion and focusing of the initial phase pP will affect m_b measurements since this arrival, in general, constructively interfers with the first backswing of the seismometer impulse response function.

3. Climax Stock - Piledriver and Hard Hat

3.1 Introduction

This report is the second part of a continuing project to define both the teleseismic path averaged attenuation operator appropriate for sources located at NTS and the deviation from the average associated with distinct geologic structures. In the first quarter (Hadley, 1979) we utilized strong ground motion records to quantify the source description for the NTS test Jorum. Synthetic teleseismic waveforms were next calculated from the resulting reduced displacement potential (RDP). Finally, through a comparison of the data with the synthetics, a path averaged attenuation operator with $t^* = 1.3$ was obtained.

As with the Jorum study, we have again tried to relate the near-field and teleseismic data for the test Piledriver (yield ~ 62 kt; Murphy, 1978b). Data from a second event, Hard Hat (yield ~ 5.9 kt; Murphy, 1978b) were also examined as a check on the Piledriver results. Hard Hat was located within the Climax Stock and was separated in distance from Piledriver by about three hundred meters. Although this shot was much too small to be recorded by the WWSSN array, both Hard Hat and Piledriver were well recorded by the short period Benioff instruments operated in southern California (Δ ~ 500 km) by Caltech. In the following sections we will interrelate: (1) near-field data from Piledriver; (2) scaling relations for a 62 kt source;

(3) teleseismic WWSSN waveforms for Piledriver; (4) regional amplitude data from Piledriver; (5) RDP's from Hard Hat; and (6) regional amplitude data from Hard Hat.

Unfortunately, these six data sets are not internally consistent. Therefore the results must depend, to some extent, on which data are heavily weighted in the analysis.

3.2 Data Analysis and Discussion

Piledriver was well recorded in the near-field by several instruments located at distances from the working point of 200 to 860 meters (for discussion see Murphy, 1978b). Two stations, Δ = 204 and 470 meters, were located well within the body of the Climax Stock. The other recording points were located either in the granite but juxtaposed to a major vertical boundary separating granite from sediments, or in the valley tuff sequence. From a simple consideration of the reflection and transmission coefficients for this boundary, data from these stations should be either contaminated by reflections from the boundary or significantly altered in transmission. Accordingly, the effort to define an RDP for Piledriver focused on the two velocity records from Δ = 204 and 470 meters, as described by Perret, (1968), Obtaining the RDP from the velocity records is straightforward and is only briefly outlined here. The displacements are related to the RDP ($\psi(t-R/\alpha)$, where R = Distance and α is P-wave velocity (taken from Murphy, 1978b, as 5.3 km/sec) by

$$U = \frac{-\partial\psi/R}{\partial R} = \frac{1}{R^2}\,\psi + \frac{1}{R\alpha}\,\frac{d\psi}{dt} \qquad (3.1)$$

The velocity is:

$$V = \frac{1}{R^2}\,\frac{d\psi}{dt} + \frac{1}{R\alpha}\,\frac{d^2\psi}{dt^2} \qquad (3.2)$$

The displacement history is obtained by integrating the velocity. Finally the RDP is defined by

$$\psi\,(t) = e^{-\frac{\alpha}{R}t}\int e^{\frac{\alpha}{R}t'}\,(\alpha R)\;U(t')dt' \qquad (3.3)$$

An example of the progression from velocity to displacement to RDP for the record at Δ = 470 meters is shown in Figure 3.1. A comparison between the two RDP's from 470 and 204 meters is shown in Figure 3.2. Although these two RDP's have different long time asymptotes, ψ_∞, the maximum value, 70-75,000 m^3, and the rise time to the maximum are very similar. The teleseismic waveforms are primarily sensitive to the rise time, maximum value and presence of an overshoot. However, as the teleseismic amplitudes are only weakly dependent on ψ_∞, the waveforms predicted from these two RDP's differ in absolute amplitude by only 10% from the average of the two.

The two velocity records, Δ = 204, and 470 meters, have been extremely important data in the comparison between finite difference calculations and observations (see for example Bache et al., 1975). Implicit in these calculations is the assumption that

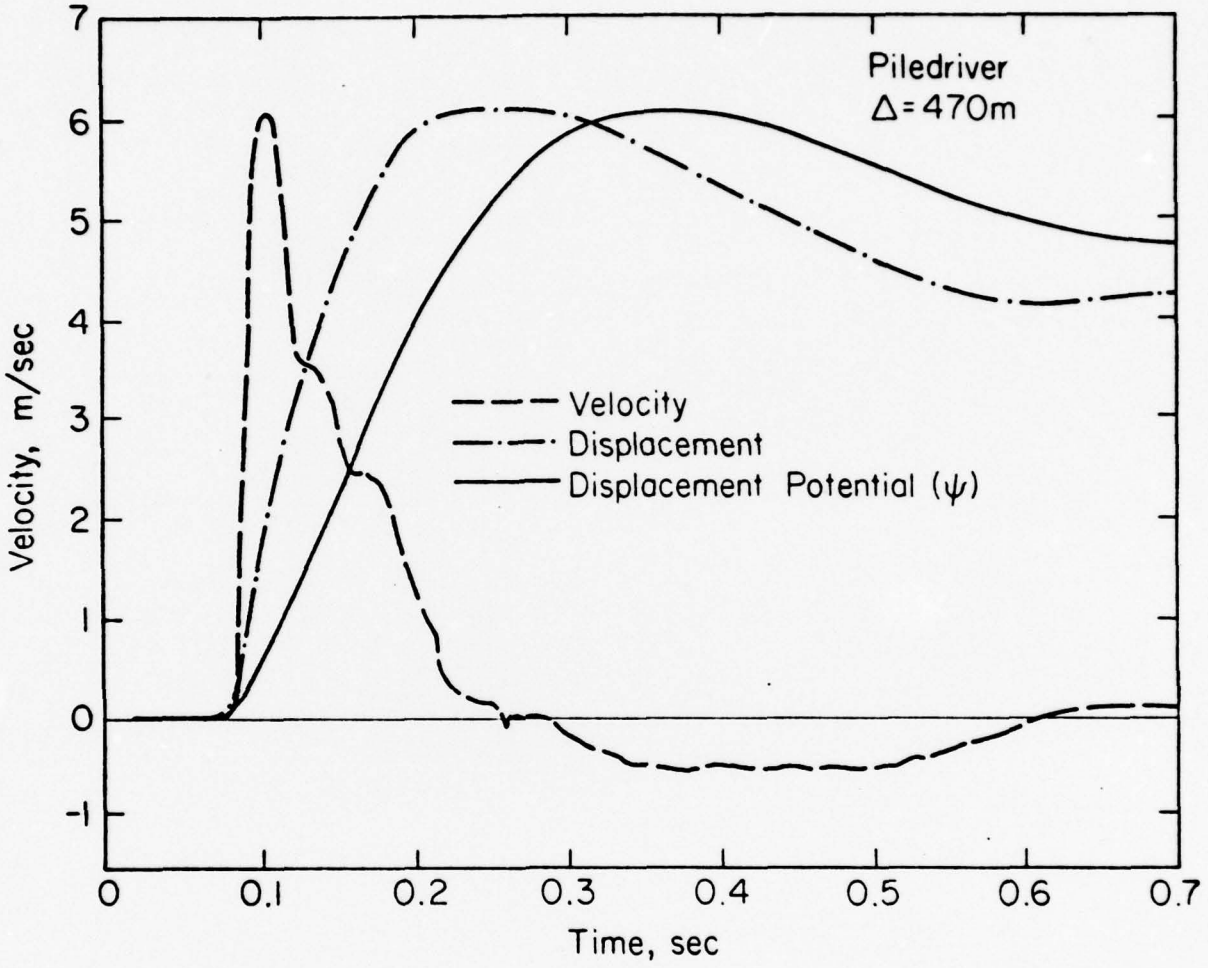

Figure 3.1. Observed velocity time history (Perret, 1968) from Piledriver (Δ = 470 m). The displacement time history is the integral of the velocity. The reduced displacement potential has been calculated from the displacements using equation 3.3 and a P-wave velocity of 5.3 km/s.

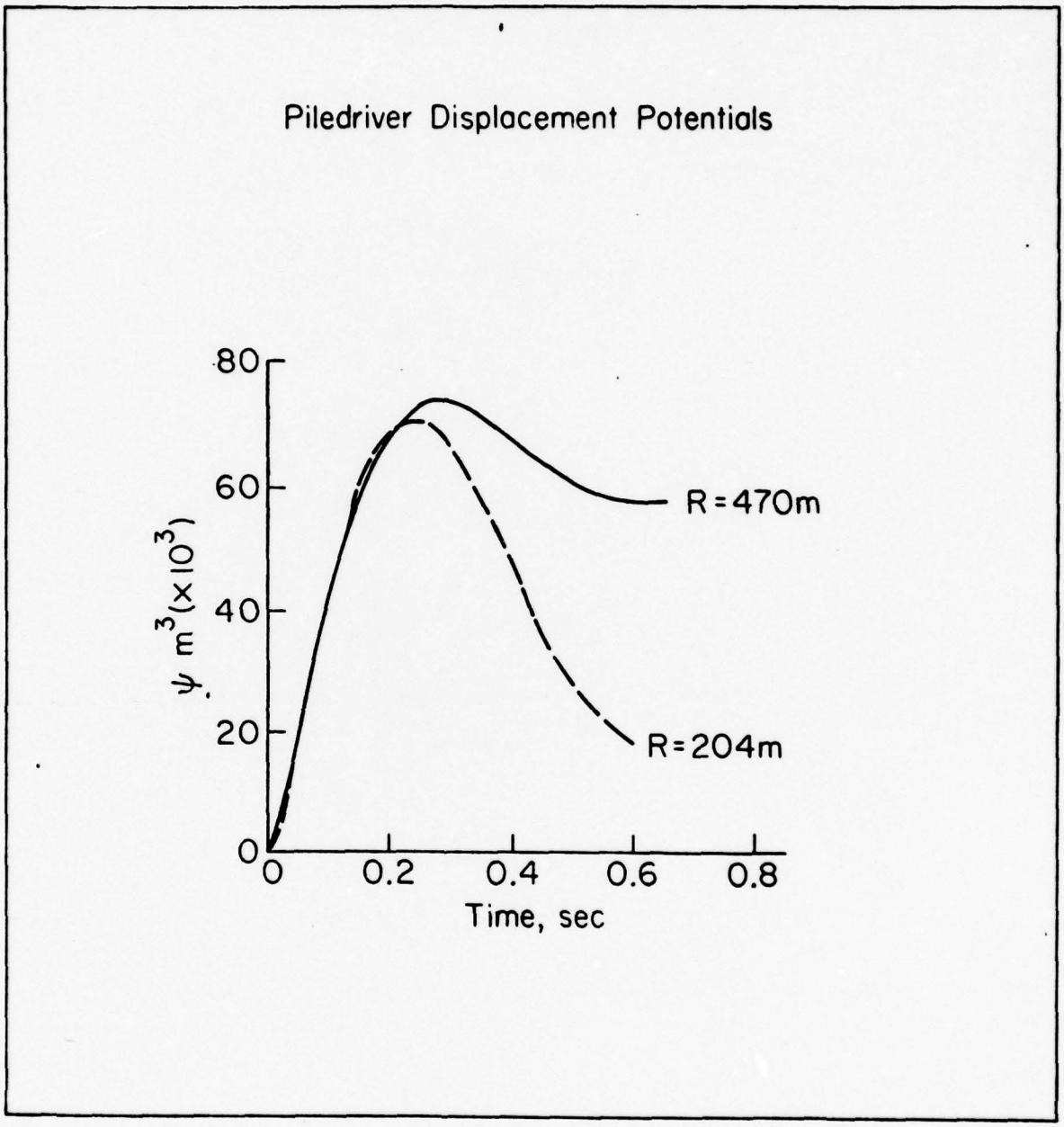

Figure 3.2. Comparison of RDP's calculated from the two velocity time histories that were recorded in the Climax Stock Granite for Piledriver. Note that the peak amplitude and rise time for these two RDP's are in good agreement.

these records are accurate representations of the whole space, elastic and non-elastic, medium response. In the Bache et al., (1975) study, the 470 meter velocity record was modeled. The resulting synthetic velocity time history was next used to compute an equivalent elastic source or RDP by using a method similar to that outlined above. This RDP was then used to calculate teleseismic waveforms. A Q operator, $t^* = 1.05$, was found to bring the calculations into agreement with the data. Using the synthetic velocity time history to calculate an equivalent elastic source implies that the distance $\Delta = 470$ meters is approximately at or greater than the elastic radius for Piledriver. For comparison with the RDP calculated directly from the observations, we have calculated an RDP from the Bache et al., (1975) synthetic velocity trace, Figure 3.3. In the comparison of Figure 3.3 with 3.2, the RDP calculated from the synthetic is about a factor of 2 smaller than the observations. However, as mentioned in the introduction and discussed in the following paragraphs, it is not obvious which RDP, synthetic or observational, is a more accurate elastic representation of the source.

The source description for Piledriver can be compared, via several scaling techniques, to the experiences from other tests. This scaling comparison rests on the assumption that the other RDP's are accurate source descriptions and that the scaling techniques are adequate. The Haskell (1967) source description as modified by von Seggern and Blandford (1972), is

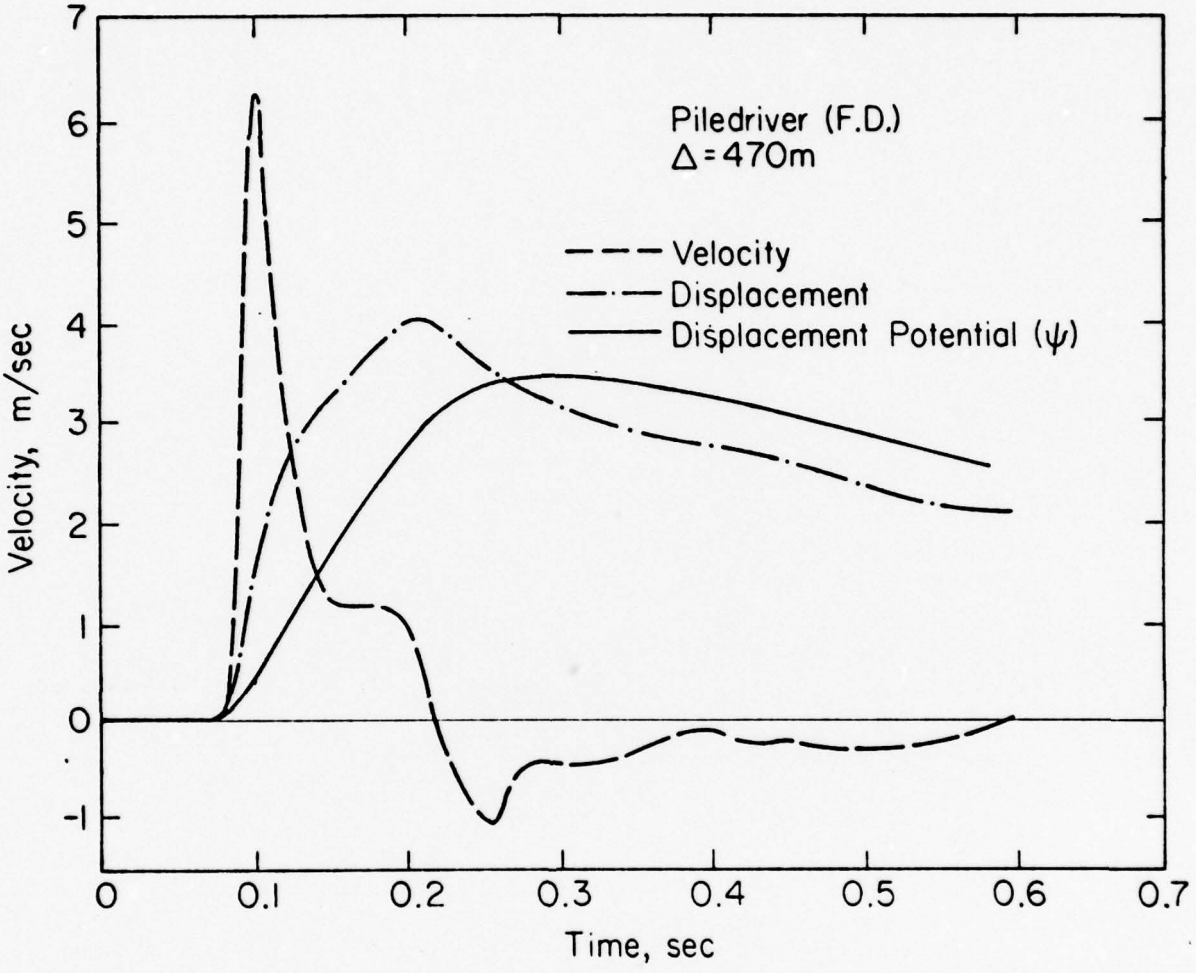

Figure 3.3. Synthesized velocity time history (Bache et al., 1975) for a station located 470 meters from the working point. The displacement and reduced displacement potential have been calculated as discussed in the text. A P-wave velocity of 5.3 km/sec has been assumed in the calculations. Note that the amplitude of this RDP is approximately 50% of that calculated from the data, Figure 3.2.

$$\psi(t) = \psi_\infty(1 - e^{-Kt}(1 + KT - B\,(Kt)^2) \qquad (3.4)$$

where the time scale K scales as $(\text{yield})^{-1/3}$ and ψ_∞ scales linearly with yield. For the four shots Hard Hat, Shoal, Piledriver and Jorum, the overshoot parameter B should be approximately constant (Haskell, 1967) and therefore the maximum value of the RDP should scale with yield. Table 3.1 shows the intercomparison of these four events. The rise time to the maximum of the RDP, scaled with respect to Hard Hat, is in good agreement with the observations for the other three tests. However, if Piledriver had a yield of 100 kt, this parameter would only change to 0.31 sec. The last column of Table 3.1, is the ratio of the maximum value of the RDP to yield. For approximately constant B, this ratio should be fairly stable. In this comparison the source strength for Piledriver, or maximum of the RDP, is about a scale factor of 2 larger than the other tests. Through a significantly more complex scaling procedure, Murphy (1978a) has predicted an RDP for Piledriver based on observations from Shoal. Murphy's predicted RDP is in agreement with the smallest RDP from Piledriver, (station was located in the tuff sequence) and is about a factor of 3 smaller than the RDP's shown in Figure 3.2. On the basis of these scaling relations, the RDP's from the three granite shots derived from the stations located in the granite, are not mutually consistent.

TABLE 3.1. SCALING RELATION FOR THE REDUCED DISPLACEMENT POTENTIAL

EVENT	Y[1] YIELD KT	OBSERVED[1] RDP RISE-TIME	OBSERVED[1] ψ_{max} x 10^3 m^3	SCALED[2] RDP RISE-TIME	RATIO $\psi_{max/Y}$
Hard Hat	5.9	.12	3.6	.12	.61
Shoal	13	.15	6.6	.15	.51
Piledriver	62	.28	73	.26	1.18
Jorum	1000[3]	.62	576	.66	.58

1. From Murphy, 1978b
2. Scaled with respect to Hard Hat
3. From Springer and Kinnaman, 1971

3.3 Far-Field Observations

Piledriver was well recorded by the WWSSN array. These teleseismic recordings are shown in Figure 3.4. In general, the recordings are fairly simple and the amplitudes, relative to the noise, are very large. However, for a small range of azimuths the waveforms are very complex and the signal strength is reduced by a factor of about 5. From the previous study of Jorum, we expect some complexity at each station to be introduced by the local receiver function and some scattering in the amplitudes from real teleseismic path differences. For comparison with Piledriver, waveforms and amplitudes from both tests are shown on a geologic map of Climax Stock, Figure 3.5. The lines leaving the working point show the great circle azimuth to each station. The amplitude ratio of Piledriver to Jorum, for stations ARE, KIP, SHK, COL, AKU, and STU is 0.30. Data from station SHK for Piledriver is somewhat small, but the signal to noise ratio is not as good for this record and the measurement may be biased. Waveforms for these stations, from both events, are relatively simple For the range of azimuths 46° to 71°, stations TOL, WES, OGD, and SCP, the waveforms from Piledriver show great complexity compared to Jorum. The averaged amplitude ratio is reduced to 0.08. These data suggest that the deep structure of the Climax Stock, along a northeast azimuth from Piledriver, is significantly altering outgoing seismic energy. The spatial coincidence of the Boundary Fault to these paths is very suggestive that the distorting structure is associated with this fault.

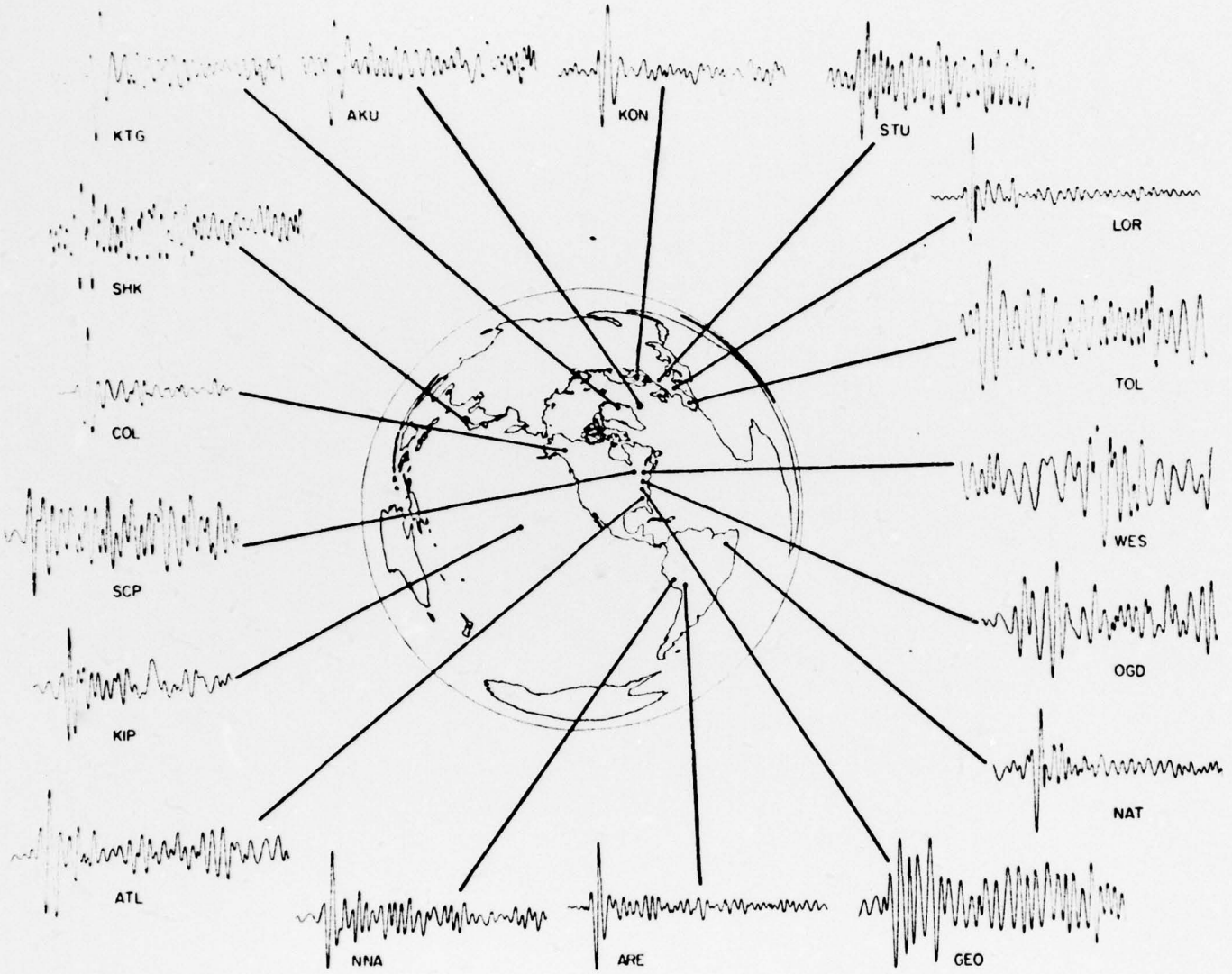

Figure 3.4. Teleseismic waveforms observed for the test Piledriver. Amplitude information is listed in Table 3.2. Note that for many stations, the waveforms are both very coherent and simple.

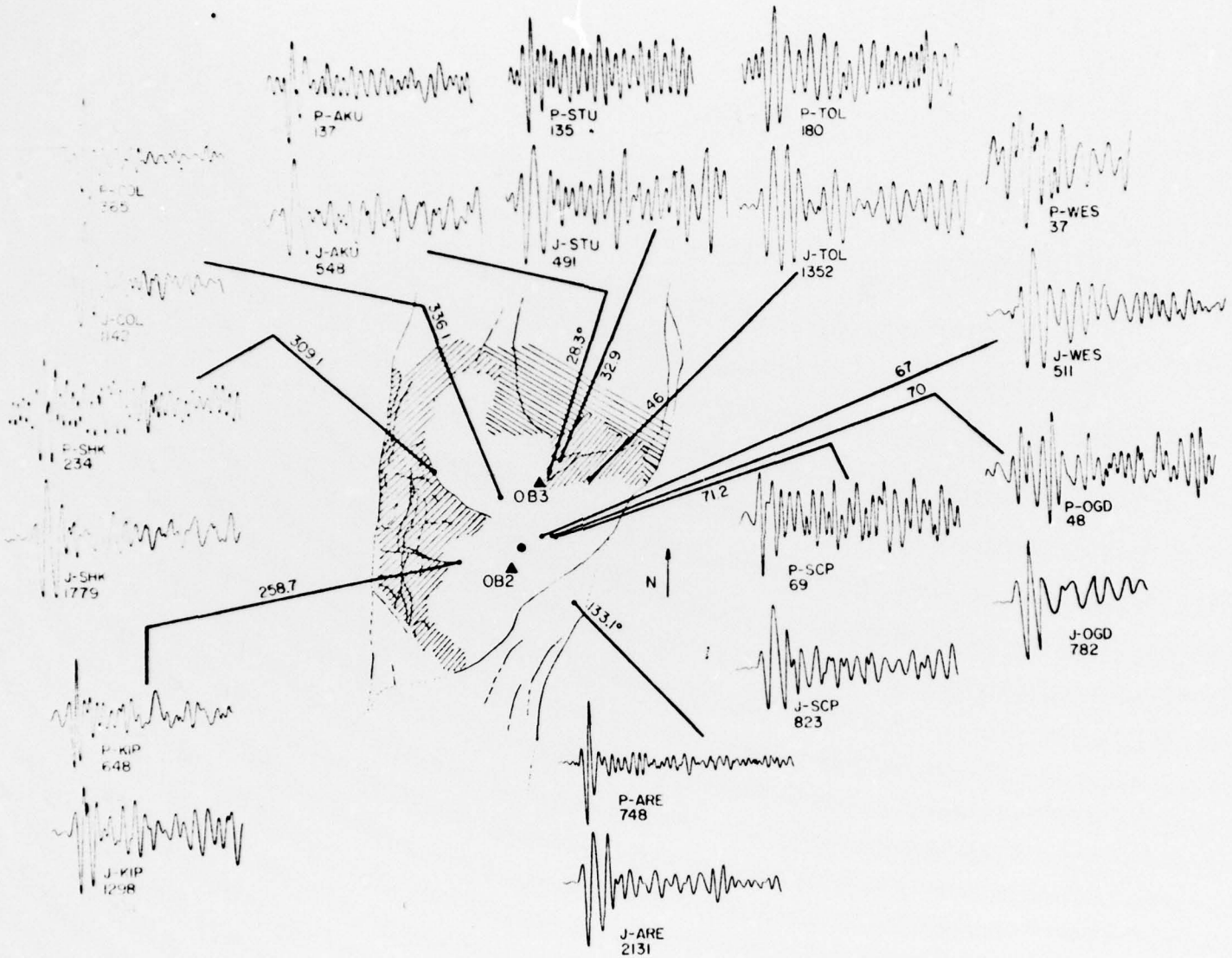

Figure 3.5. Comparison of the waveforms and amplitudes from Piledriver (P) and Jorum (J). Generalized map shows the Climax Stock, location of the SDCS stations OB2NV and OB3NV and the location of Piledriver (dot north of OB2). Lines radial from Piledriver show the great circle azimuth to the WWSSN stations. Excluding stations TOL, WES, SCP, and OGD, the average amplitude ratio is 0.30. Amplitude and waveforms for these four stations, for Piledriver relative to Jorum, are both attenuated (average ratio = 0.08) and distorted. These data suggest that the deep structure of the Climax Stock, along a northeast azimuth from Piledriver is significantly altering outgoing seismic energy.

The various RDP's discussed in the first section are easily used to calculate teleseismic waveforms. Figure 3.6 shows the shape and amplitude of the far-field displacement pulse calculated from both the observed velocity data, Figures 3.1 and 3.2, and the finite difference calculation, Figure 3.3. The area of the two pulses differs by about a factor of 2 and for given value of t* (= 1/05 to 1.3) the teleseismic amplitude ratios differ by a similar factor. Figure 3.7 shows waveforms for two values of t* (1.0 and 1.3) for these different RDP's. From the observed amplitude data, Table 3.2, the amplitude of the synthetics should be adjusted to a value of about 270 mμ. The average amplitude, assuming a t* = 1.3 computed from the observed velocity records, Figure 3.2, is 270 mμ. The amplitude of the waveforms computed from the synthetic velocity pulse (Bache et al., 1975 labeled S^3) for t* = 1.0 is 360 mμ. If the finite difference calculations adequately characterize the source, the t* value of 1.05 reported by Bache et al., (1975) is here simply reconfirmed.

The amplitude of the teleseismic waveforms are very sensitive to the arrival time of the phase pP. Within this study, pP has been lagged in time by 0.16 sec. from the direct arrival. This time was computed from the source depth, the velocity structure (summarized by Murphy, 1978b) and the ray parameter. From Figure 3.6 the width of the far-field pulse is about 0.25-0.3 sec. The phase pP therefore effectively cancels out part of the direct arrival.

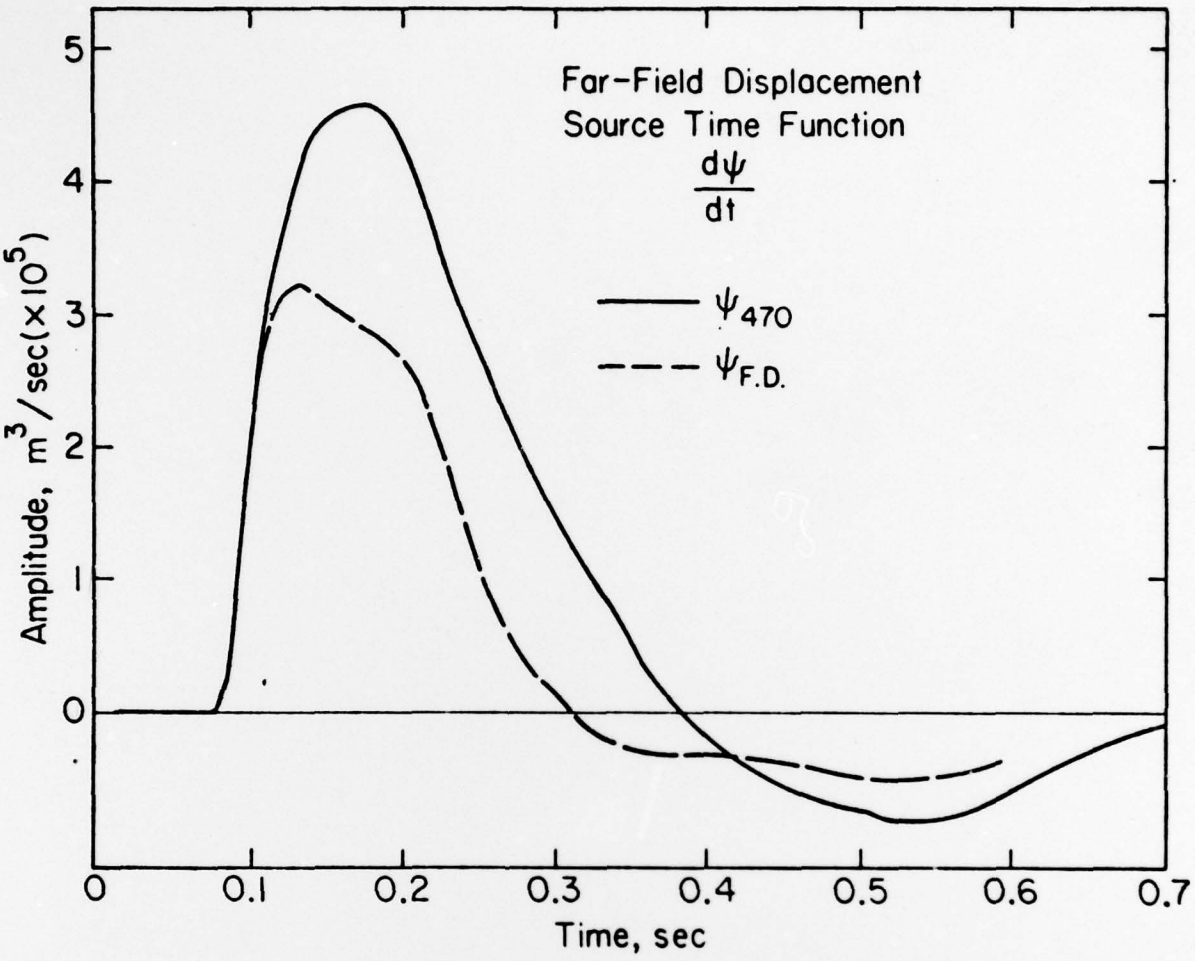

Figure 3.6. Far-field displacement time function, $d\psi/dt$, calculated from RDP's shown on Figure 3.1 (ψ_{470}) and Figure 3.3 ($\psi_{F.D.}$). The area of these two pulses differ by about a factor of 2.

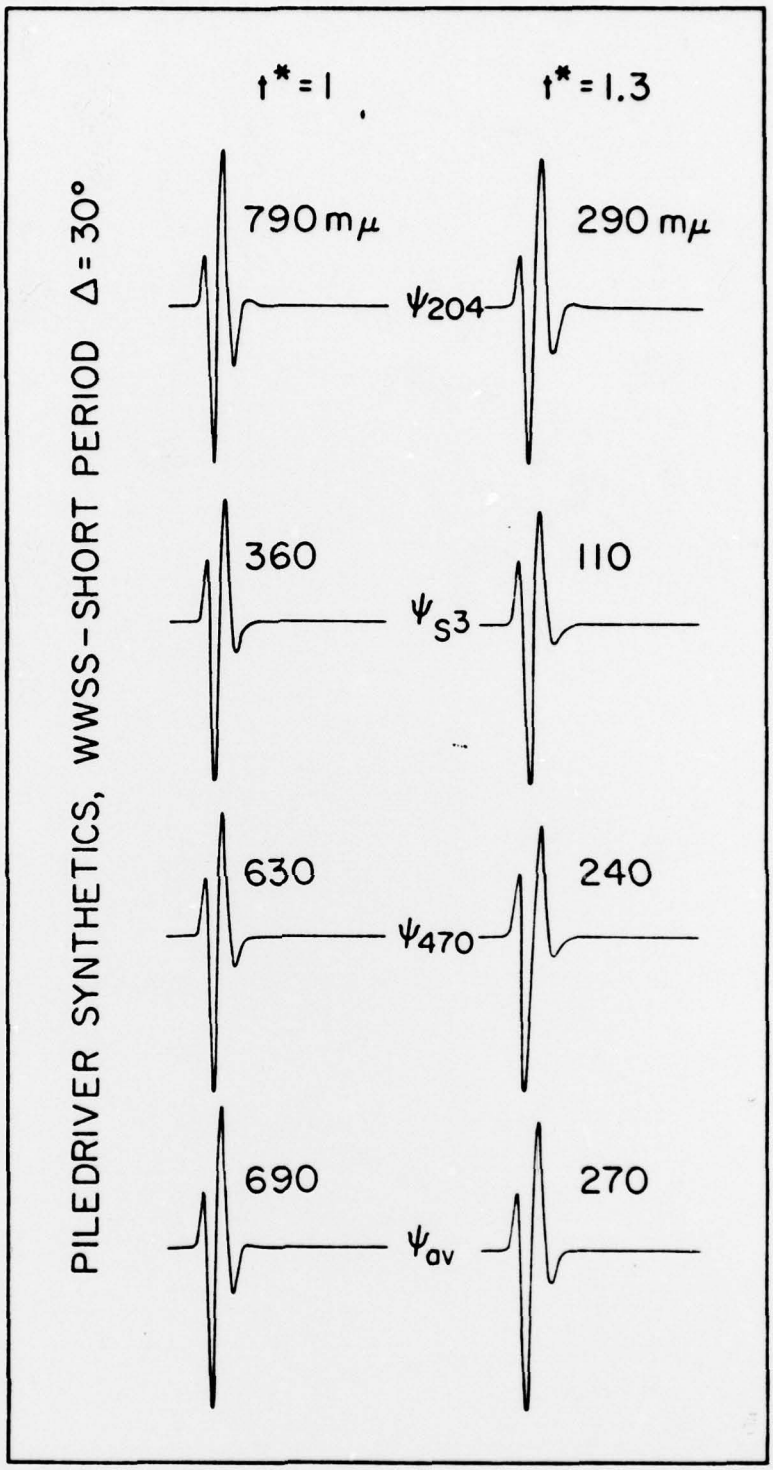

Figure 3.7. Teleseismic synthetic waveforms and amplitudes calculated from RDP's shown on Figure 3.2 (ψ_{204}, and ψ_{470} and $\psi_{average}$) and Figure 3.3 ($\psi_S 3$). The average amplitude from the WWSSN data, Table 3.2, is ~ 270 m . For ψ_{204}, ψ_{470} and the average of the two, ψ_{av}, a value of t* = 1.3 is very compatible with the data. For the $\psi_S 3$ RDP, a t* value slightly greater than 1 would also be consistent with the data.

TABLE 3.2. PILEDRIVER TELESEISMIC AMPLITUDES

STATION	AMP (mμ)	C.AMP (mμ)[1]	STATIONS EXCLUDED
SCP	69	69	x
OGD	46	48	x
GEO	103	108	
ATL	171	160	
COL	343	365	
WES	34	37	x
KIP	548	648	
NOR	183	256	
KTG	91	101	
AKU	91	137	
NNA	171	261	
ARE	446	748	
TOL	91	180	
STU	69	135	
SHK	114	234	
NAT	183	284	
KOM	183	301	
LOR	177	291	
UME	171	281	
		$\overline{A} = \overline{244}$	$\overline{A} = \overline{280}$ mμ[2]

1. Corrected for geometric spreading

2. Three smallest amplitudes were excluded from the average.

If the shallow velocity structure during the shot was perturbed such that pP arrived about 0.25 sec. behind P, then the teleseismic amplitude would increase by 48%, Figure 3.8.

The event Hard Hat was too small to be recorded at many of the WWSSN stations (in addition the array was not entirely functional). However it was well recorded by several instruments operated by Caltech. Most of the seismographs were of the short period Benioff design. Several excellent records were also written by special long-period instruments located at Pasadena. The same suite of instruments recorded the Piledriver test. The amplitudes of the first peak and/or first peak to first trough were read for each pair of records from each station. These ratios and a qualitative estimate, ranging from A to C, of the quality of the records are listed in Table 3.3. The average Piledriver to Hard Hat amplitude ratio is about 7. The RDP's from both Hard Hat and Piledriver have been discussed above. Computing the relative amplitudes for the regional synthetic records requires several additional assumptions. The first arrival at all stations is P_n. We assume the transfer function for this arrival represents a slightly diving ray and is therefore a delta function. In addition, we assume an average Q of 500-600. Increasing Q will decrease to some extent the synthetic Piledriver/Hard Hat ratio. A low Q quickly attenuates the short duration high frequency energy from Hard Hat and dramatically increases the ratio. As in the teleseismic case, changing the

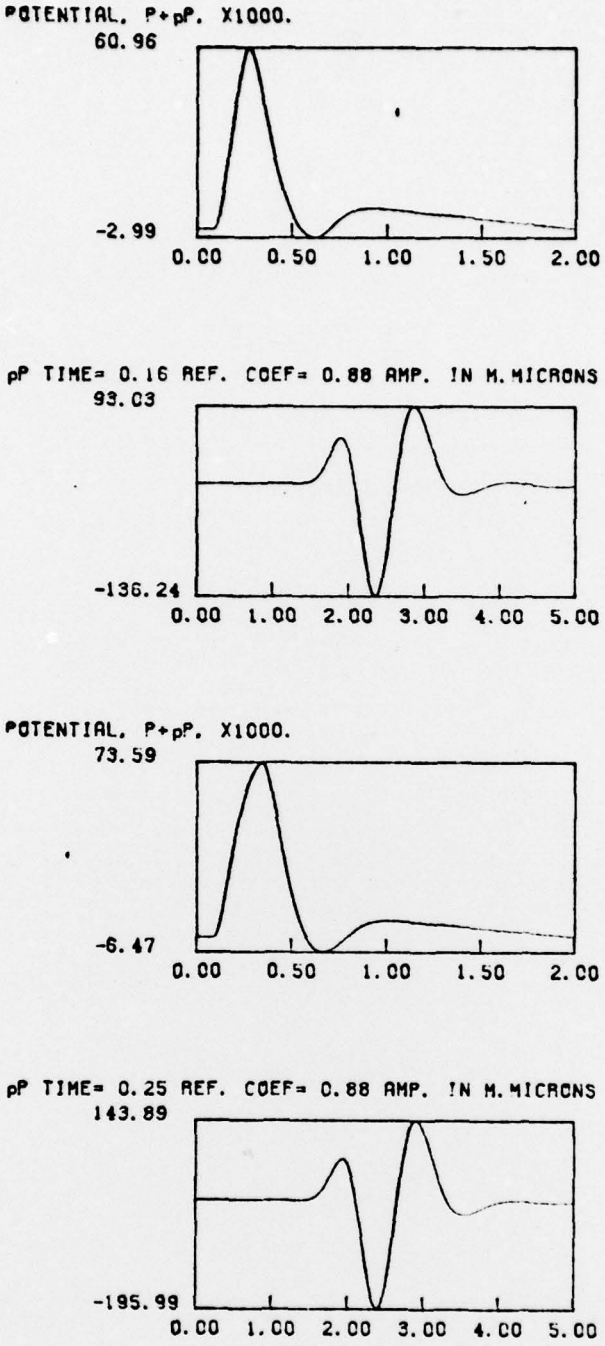

Figure 3.8. Effect on the amplitude of synthetic seismograms resulting from changing pP arrival time from 0.16 to 0.25 sec.

TABLE 3.3. Ratio of P_n amplitudes for Piledriver/Hard Hat. Measurements were made of the amplitude of the first peak and of the first peak to first trough. These stations are located in southern California (Δ ~ 500 km) and operated by Caltech.

STATION	COMPONENT	RATIO	QUALITY P.D./H.H.
PLM	SPZ	4.7	A/A
PAS	N-S-31	5.0	A/B
PAS	N-S-20	6.8	A/B
PAS	Z-16	8.3	A/A
HAY	SPZ	10.6	B/B
		7.1	C/C
MWC	SPZ	6.7	A/C
		6.6	B/A
RVR	SPZ	8.5	A/B
TIN	E-W	6.9	A/A
FTC	SPZ	5.3	A/B

$\bar{x} = 6.95 \pm 1.7$

lag time for pP can very effectively cancel out the source strength and dramatically change the amplitude ratio. Based on the velocity data and ray parameter appropriate for P_n, we have used a pP time of 0.14 sec. for Piledriver and 0.10 for Hard Hat. From these many assumptions, the synthetic Piledriver/Hard Hat ratio, computed from the RDP's obtained from the near-field data, is about 12. Since these two shots are located about 300 meters apart, both in the Climax Stock granite, presumably the coupling was approximately equivalent. From the comparison with the regional data (ratio = 7, Δ ~ 500 km) we must conclude that the RDP's from Hard Hat (from Murphy, 1978b) and Piledriver (derived from velocity records Δ = 204 and 470 meters) are not mutually compatible.

If we accept the scaling arguments, we suspect the RDP's derived from the near field velocity data are too large. By decreasing the maximum of the RDP by a factor of 2, the agreement with the scaling for Hard Hat and Shoal would be improved and the regional comparison between Piledriver and Hard Hat would be compatible with the observations. For this decreased RDP, a t* value of 1.0 to 1.1 would bring the amplitude of the synthetics into agreement with the data. This value is significantly lower than the value of 1.3 found from the study of Jorum, located in the Silent Canyon Caldera. The higher attenuation from the Jorum measurements may be the result of either intrinsic attenuation associated with the old Caldera or effective attenuation introduced

by geometric spreading at curved velocity gradients in the crust or upper mantle.

On the other hand, rejecting the near field velocity data from Piledriver in favor of Hard Hat and Shoal is somewhat ad hoc. A persuasive argument for accepting either data set as truly representing the source is lacking. Because of these inconsistencies in the data, we cannot, at this time, assign with great confidence any t* value for the sources located within the Climax Stock. Through careful modeling of the near surface amplification for the two SDCS stations OB2NV (on Climax Stock) and NTNV (Silent Canyon Caldera), incoming teleseisms should provide a data set that can resolve real differences in near station attenuation.

REFERENCES

Bache, T. C., T. G. Barker, N. Rimer, T.R. Blake, D. G. Lambert, J. T. Cherry, J. M. Savino, (1975). An explanation of the relative amplitudes of the teleseismic body waves generated by explosions in different test areas at NTS, DNA, 3958F.

Choy, G. L. and P. G. Richards, (1975). Pulse distortion and Hilbert transfromation in multiply reflected and refracted body waves, Bull. Seism. Soc. Am., 65, 55-70.

Hadley, D.M., (1979). Seismic source functions and attenuation from local and teleseismic observations of the NTS events Jorum and Handley, AFTAC Quarterly Technical Report, Sierra Geophysics, Inc.

Haskell, N.A., (1967). Analytic approximation for the elastic radiation from a contained underground explosion, Journal Geophysical Res., 72, 2583-2587.

Murphy, J. R., (1978a) Seismic coupling and magnitude/yield relations for underground nuclear detonations in Salt, Granite, Tuff/Rhyolite and Shale emplacement media, Interim Technical Report, AFTAC, (SECRET).

Murphy, J. R., (1978b). A review of available free-field seismic data from underground nuclear explosions in Salt and Granite, Computer Sciences Corp., CSC-TR-78-0003.

Perret, W. R., (1968). Free field ground motions in Granite, operation flint rock, shot Piledriver, DASA POR - 4001.

Springer, D. L. and R. L. Kinnaman, (1971). Seismic source summary for U.S. underground explosions, 1961-1970, Bull. Seism. Soc. Am., 61, 1073-1098.

von Seggern, D., and R. Blandford, (1972). Source time functions and spectra for underground nuclear explosions, Geoph. J. Roy. astr. Soc. 31, 83-98.